Kinetics and Thermochemistry of the Hydroxycyclohexadienyl Radical Reaction with O_2: $C_6H_6OH + O_2 \rightleftharpoons C_6H_6(OH)OO$

Sergey Y. Grebenkin and Lev N. Krasnoperov*

Department of Chemistry and Environmental Science, New Jersey Institute of Technology, University Heights, Newark, New Jersey 07102

Received: July 30, 2003; In Final Form: December 18, 2003

The UV absorption spectrum along with the self-reaction and oxidation reaction kinetics of the hydroxycyclohexadienyl radical, C_6H_6OH (which results from OH addition to benzene), were studied using excimer laser photolysis coupled to transient UV absorption. The radicals were generated by photolysis of $N_2O/H_2O/C_6H_6$/He mixtures at 193 nm in a series of chemical reactions initiated by $O(^1D)$. The radical has continuous absorption in the range 260−340 nm with a maximum absorption cross-section of $(8.1 \pm 1.4) \times 10^{-18}$ cm^2 molecule^{-1} at 280 nm. Reaction of the radical with molecular oxygen, $C_6H_6OH + O_2 \rightleftharpoons C_6H_6(OH)OO$ (1), and self-reaction $C_6H_6OH + C_6H_6OH \rightarrow$ products (2), were studied over the 252−285 K temperature range at 1.01 ± 0.02 bar (He). The radical temporal profiles were recorded via transient absorption at 315 nm. In reaction 1, two-time-domain "equilibration" kinetics were recorded in the temperature range 252−273 K. The rate constant of the addition reaction is $k_1 = (1.4 \pm 0.8) \times 10^{-12} \exp(-18.6 \pm 1.7 \text{ kJ mol}^{-1}/RT)$ cm^3 molecule^{-1} s^{-1}. The standard enthalpy of reaction 1 was determined from the measured equilibrium constants using the third law method: $\Delta H^\circ_{298} = -43.6 \pm 2.0$ kJ mol^{-1}. The measured rate constant of self-reaction 2 is $k_2 = (6 \pm 3) \times 10^{-11} \exp(-2.00 \pm 1.6 \text{ kJ mol}^{-1}/RT)$ cm^3 molecule^{-1} s^{-1}.

Introduction

Reaction of hydroxycyclohexadienyl radical, C_6H_6OH (which results from OH addition to benzene), with molecular oxygen

$$C_6H_6OH + O_2 \rightleftharpoons C_6H_6(OH)OO \quad (1)$$

is the major transformation route of these radicals in the atmosphere.[1−4] Due to the relatively weak chemical bonding of the oxygen molecule in the adduct ($DH^\circ_{C_6H_6(OH)-OO}$ is estimated as 48 kJ mol^{-1} [2]), the formation of the hydroxycyclohexadienyl peroxy radical, $C_6H_6(OH)OO$, is reversible near ambient conditions. At higher concentrations of free radicals, as exist in the laboratory measurements, self-reaction 2 of hydroxycyclohexadienyl radicals is another important transformation route:

$$C_6H_6OH + C_6H_6OH \rightarrow \text{products} \quad (2)$$

The hydroxycyclohexadienyl radical, C_6H_6OH, is an important intermediate in the oxidation of atmospheric aromatic hydrocarbons.[2−10] In the atmosphere, hydroxycyclohexadienyl radicals are formed via addition of hydroxyl radical to benzene:

$$C_6H_6 + OH \rightarrow C_6H_6OH \quad (3a)$$

$$C_6H_6 + OH \rightarrow C_6H_5 + H_2O \quad (3b)$$

The H-atom abstraction route 3b is a minor process at atmospheric conditions.[10−12]

Despite the importance of C_6H_6OH radicals in the oxidation of benzene, they are not well studied. There are several important issues relevant to the characterization of the spectroscopy and reactivity of the hydroxycyclohexadienyl radical, which are still poorly resolved. These include the rate constant of reaction 1, the R−OO bond in the hydroxycyclohexadienyl peroxy radical, as well as the shape of the absorption spectrum and the absolute UV absorption cross-section of the hydroxycyclohexadienyl radical.

The rate constant of reaction 1 has been measured in several experimental studies.[1,9,11] The measured rate constants of this reaction [$k_1 = (1.8 \pm 0.5) \times 10^{-16}$ at 298 K,[9] $(5.0 \pm 1.0) \times 10^{-13}$ at 338 K,[11] and $(2 \pm 1) \times 10^{-15}$ at 297 K[1] (cm^3 molecule^{-1} s^{-1} units)] differ by a 3 orders of magnitude.

The R−OO bond energy in the peroxy radical which is formed in reaction 1 was estimated as $DH^\circ_{298} = 48$ kJ mol^{-1} based on the group additivity approach and semiempirical (PM3) method.[2] This bond energy combined with the estimated standard entropy of reaction 1 of $\Delta S^\circ_{298} = -136$ J mol^{-1} K^{-1} [2] implies reversibility of reaction 1 near ambient conditions. The higher level calculations of Ghigo and Tonachini (DFT-B3LYP/6-31G+G(d))[13,14] resulted in a much smaller bond energy in the peroxy adduct, only ca. 5 kJ mol^{-1},[13] which implies a complete shift of the equilibrium toward the reactants in reaction 1 and unimportance of the peroxy radical as an individual chemical species near ambient conditions. The standard Gibbs energy of reaction 1, $\Delta G^\circ_{298} = 44$ kJ mol^{-1}, calculated by Ghigo and Tonachini[14] corresponds to a very small thermodynamic equilibrium constant for reaction 1, $K_{1,298} = 2 \times 10^{-8}$ (which corresponds to $K_{c1,298} = 8 \times 10^{-28}$ cm^3 molecule^{-1}). Recent theoretical calculations of Johnson et al.,[15] CCSD(T)/6-31G(d,p)), $DH^\circ_{298} = 51$ kJ mol^{-1}, and Chen and Bozzelli,[16] G3MP2, $DH^\circ_{298} = 56$ kJ mol^{-1}, are consistent with the initial estimates[2] and confirm the importance of the peroxy intermediate. The recent theoretical calculations indicate the (*E*)-ortho-hydroxycyclohexadienyl peroxy radical as the most stable isomer among the possible adducts produced in reaction 1.[15,16]

* To whom correspondence should be addressed. E-mail: krasnoperov@adm.njit.edu.

10.1021/jp030935c CCC: $27.50 © 2004 American Chemical Society
Published on Web 02/21/2004

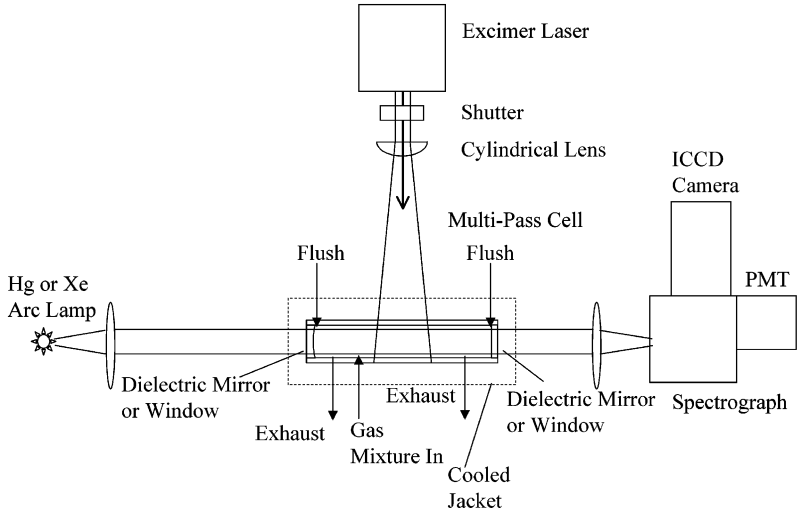

Figure 1. Experimental setup.

Bohn and Zetzsch[1] monitored decay of hydroxycyclohexadienyl radicals by absorption at 308 nm. Hydroxycyclohexadienyl radicals were produced by addition of hydroxyl radicals (produced in photolysis of hydrogen peroxide at 248 nm) to benzene. In the presence of molecular oxygen, a decrease in the amplitude of benzene−OH (the hydroxycyclohexadienyl radical) absorption was observed. This decrease of the "initial" radical concentration was interpreted as being due to the fast (below the time resolution) equilibration in reaction 1. The first stages of the equilibration kinetic curves were not resolved in these experiments. The equilibrium constant for reaction 1 was obtained (assuming a small reaction mechanism) at a single temperature, 298 K: $K_{c1,298} = 2.7 \times 10^{-19}$ cm^3 molecule^{-1}.

Johnson et al.,[15] using the same photochemical generator of hydroxycyclohexadienyl radicals as Bohn and Zetzsch and transient UV absorption, studied the equilibrium in reaction 1 over the temperature range 265−345 K. The decrease in the transient absorption under the addition of molecular oxygen was again interpreted in terms of the equilibrium in reaction 1, but the complete equilibration curve was, however, still not resolved. The equilibrium constant extrapolated to 298 K implies $K_{c,1,298} = (8.0 \pm 0.6) \times 10^{-20}$ cm^3 molecule^{-1}, a factor of 3.4 lower than that measured by Bohn and Zetzsch. The temperature-dependent equilibrium constant combined with their theoretical standard entropy of reaction 1 ($\Delta S^\circ_{1,298} = -160$ J mol^{-1} K^{-1}) yielded a bond enthalpy in the peroxy radical DH° of 49 ± 1 kJ mol^{-1}.[15]

In this study, we report the results of measurements on the kinetics and thermochemistry of reaction 1 and the UV spectroscopy of the hydroxycyclohexadienyl radical. A different photochemical source of the radicals was used. Improvement in the sensitivity achieved with a novel multipass cell allowed unambiguous resolution of both components of the pseudo-equilibration kinetic curves in reaction 1. The rate constant and the equilibrium constant of reaction 1 were measured over the temperature range 252−285 K. The equilibrium constants were used to determine the bond energy in the peroxy radical. The rate constant of self-reaction (reaction 2) and the UV absorption cross-sections of the hydroxycyclohexadienyl radical were also determined.

Experimental Section

Experimental Setup. The experimental approach used in this work is based on the combination of laser pulsed photolysis with transient UV absorption spectroscopy. Details of the signal accumulation are given elsewhere.[17] A diagram of the experimental setup is shown in Figure 1. Reactant mixtures flowed continuously through an atmospheric pressure flow cell. Gas flow rates were controlled by mass flow controllers (Brooks, model 5850). The typical total flow rate was ca. 20 sccs. The low repetition rate of laser pulses (1 Hz) provided complete replenishment of the cell between the laser pulses.

Two experimental arrangements were used: one-pass and multipass absorption cells.

One-Pass Cell. The one-pass absorption cell (fused silica tube, internal diameter 7.0 mm, sampling length of 20.0 cm) equipped with two fused silica windows was used to record the transient absorption spectra. The Xe arc lamp (75 W, Oriel Instruments) was used as a monitoring light source. Light from the lamp is focused into the cell and then onto the entrance slit of a grating spectrograph (SpectraPro-300i, Acton Research Corp.) using two fused silica lenses. The spectra were recorded with spectral resolution of 1.1 nm. This cell was used with a gated intensified CCD Camera (ICCD-MAX, Princeton Instruments) to record the transient absorption spectra.

Multipass Cell. Higher sensitivity in the transient absorption measurements needed for the resolution of the two-domain equilibration kinetic profiles was achieved with a multipass cell of a novel design. The kinetic measurements were performed at a fixed wavelength, 315 nm. This cell made of a fused silica tube with the internal diameter of 7.0 mm and sampling length of 20.0 cm was equipped with two dielectric mirrors. The mirrors replace the windows used in the single-pass measurements. To avoid contact of the mirrors with the reactant mixture, the mirrors were flushed using small (additional) flows of the carrier gas. The combined flow of the flush gas was ca. 4% of the total flow. The monitoring light source (Hg arc lamp, Oriel Instruments) was placed at a distance of 1.9 m from the cell to provide better matching of the beam geometry with the multipass cell. The multipass cell was made of one flat dielectric mirror and one concave dielectric mirror with a 1.0 m radius of curvature from CVI Laser Corporation. Both mirrors have a manufacturer stated reflectivity of 99.0 ± 0.5% at 325 nm (the wavelength of the monitoring light in this study was 315 nm). The mirrors were mounted in angular adjustable mounts at a distance of 23 cm. In this geometry, the mirrors form an optically stable Fabry-Perot cavity (stable in the sense that an optical ray under the approximation of the geometrical optics

will never leave the cavity). The increase in the sensitivity is achieved due to the multiple reflections of the monitoring light inside the cell. A simple theory (see the Appendix) implies that the "gain" of the cell (defined as the average number of passes of a photon of the monitoring light inside the cell) is given by the following simple expression:

$$\text{Gain} = \text{One Pass Loss}^{-1} \qquad \text{(E1)}$$

where "One Pass Loss" is the one pass loss of the cavity at the monitoring wavelength. Equation E1 is valid provided that all of the modes excited in the cell have equal one-pass losses. In practice, this suggests that the coupling of the cell with the monitoring light source should exclude excitation of the high transverse modes, which have the diffraction losses comparable with the mirror losses. Expression E1 predicts a maximum expected theoretical gain of 100 for mirrors with 99% reflectivity. The actual gain differs due to the deviation of the reflectivity of the mirrors from 99% and due to the imperfect coupling of the monitoring beam with the cavity. It was found empirically that the coupling (evaluated via the cell gain) improves when the light source together with the collimating lens is placed away from the cell. The gain of the cell was determined using absorption of the monitoring light by a stable compound, acetone. The cell calibration and the gain stability were checked routinely during the measurements. The measured cell gain ($G = 52 \pm 2$) was stable over the lifetime of the experiments within the quoted uncertainty.

A light shutter (Oriel model 76993) was located between the laser and the cell. Every alternate laser pulse was blocked. In the kinetic measurements, a signal switch synchronized with the shutter (Pasternack Electronics, PE7100) was used to alternately send the preamplifier output to the two input channels of a digital storage oscilloscope (LeCroy 9310A). The temporal profiles of the monitoring light intensity with and without the photolytic light entering the reactor were separately accumulated. This procedure was used to remove some irrelevant signal transients (such as the electromagnetic interference from the laser, etc.) as well as to compensate for slow variations of the monitoring light intensity. The two traces were used to calculate the temporal profiles of the monitoring light absorption caused by the transient species in the cell after the signal accumulation.

A Xe arc lamp was used as the monitoring light source in measurements of the UV−vis transient absorption spectra. The light intensity spectra were recorded with and without the laser light entering the reactor by blocking alternate pulses with the shutter and storing individual ICCD frames in the computer. The ICCD gating, with a delay after the laser pulse, provided the temporal behavior of the transient absorption. The summed on and off intensity vs wavelength profiles were used as the $I(\lambda,t)$ and $I_0(\lambda)$. The ratio of these profiles was used to calculate the transient absorption spectra: $\text{Abs}(\lambda,t) = -\ln(I(\lambda,t)/I_0(\lambda))$.

A mixture of acetone (mole fraction of $(6.08 \pm 0.07) \times 10^{-3}$) in He) was used for the periodic cell calibration. The actual cell gain was determined using eq E2 (see the Appendix):

$$\text{Gain} = (1 - I/I_0)/(\sigma_\lambda\, l\, [\text{acetone}]) \qquad \text{(E2)}$$

where I and I_0 are the light intensities at the monitoring wavelength λ passing through the cell with acetone and without acetone, σ_λ is the absorption cross section of acetone at the monitoring wavelength (315 nm), and l is the optical path through the acetone vapor inside the cell.

The optical path was smaller than the distance between the mirrors due to the mirrors flush. The optical path could not be defined precisely for this cell arrangement. It is noted, however, that only the product of the absorption cross-section and the optical path, $\sigma_\lambda l$, is required for the cell calibration (more exactly, the integral of the optical density along the monitoring light beam). This product was measured in the following experiments. The dielectric mirrors were replaced with windows made of fused silica. Mixtures of acetone in helium with various acetone concentrations ($0.233 \times 10^{18}-2.43 \times 10^{18}$ molecule cm^{-3}) were flowed through the cell while the windows were flushed by helium. The distribution of the flush and the main carrier flow was identical to that in the experiments. The value of $\sigma_\lambda l = (2.78 \pm 0.13) \times 10^{-19}$ cm^3, used in the calibrations, was derived from the slope of a plot of the absorbance vs the acetone concentration. This approach allows the uncertainty of the absorption zone length in the calibration experiments to be accounted for and quantitative absorption spectra measurements to be performed. The calibration allows for the accurate determination of the cell gain. In the UV absorption cross-section measurements as well as in the kinetic measurements, the optical path was determined by the aperture used on the photolysis laser beam.

Figure 1 shows the experimental arrangement with the photolytic light entering the cell through the wall of the cell perpendicular to the propagation direction of the monitoring light. The beam from an ArF (193.3 nm) excimer laser (OPTEX, Lambda Physik) is dispersed by a cylindrical lens in the horizontal direction so that the spot size at the cell distance is 12 cm. In the measurements of the absorption spectra, the irradiated length of the cell was 10 cm (limited by an aperture), the typical photon flux was $(3.4 \pm 0.8) \times 10^{14}$ photon cm^{-2}, and the laser light intensity uniformity was ±20%. The illuminated path length was not used in the cross-section determination, and the laser light intensity nonuniformity did not add to the cross-section uncertainty, since the relative measurements were performed using the same light geometry. In the kinetic measurements, the typical photon flux was $(1.4 \pm 0.3) \times 10^{14}$ photon cm^{-2} with the intensity uniformity of ±10%. Typical initial concentrations of free radicals in the kinetic measurements were $[O(^1D)]_0 = 7 \times 10^{12}$ molecule cm^{-3}, $[C_6H_6OH]_0 = (1.0-1.5) \times 10^{12}$ molecule cm^{-3}. The initial concentration of C_6H_6OH was 4−7 times lower than the initial concentrations of $O(^1D)$ due to the quenching by N_2O and O_2 which competes with the reaction of $O(^1D)$ with H_2O.

Before entering the cell, the gas mixture passed through the cooling aluminum housing on the cell and was cooled to the cell temperature. The temperature of the housing was stabilized to ±1 °C using an OMEGA CN9000A Microprocessor Controller together with a Type K (CHROMEGA-ALOMEGA) thermocouple and a heater incorporated in the body of the housing. The cell housing was cooled by a flow of cold gaseous nitrogen obtained by steady evaporation of liquid nitrogen from a tank.

Reactants. Helium (Matheson, 3500 PSIG grade, 99.995% min.) was passed through an in-line oxygen/moisture trap (R&D, model OT2-SS). A mixture of benzene (J. T. Baker Chemical Co., Baker "Resi-Analyzed") with helium, typical mole fraction of 6.6×10^{-3}, was prepared in a 34 L tank. Benzene was degassed and used without further purification.

Nitrous oxide (Scott Specialty Gases, 99.9995%) and oxygen (Matheson, UHP, 99.98% min.) were used without further purification.

Acetone from Aldrich (99.5+%, A. C. S. reagent) was used in the cell calibration without further purification.

Generation of Hydroxycyclohexadienyl Radicals. Hydroxycyclohexadienyl radicals were produced using excimer

TABLE 1: Reaction Mechanism Used in the Data Analysis

reaction	rate constant, cm^3 $molecule^{-1}$ s^{-1}	ref
$O(^1D) + N_2O \rightarrow 2NO$	7.2×10^{-11}	18
$O(^1D) + N_2O \rightarrow N_2 + O_2$	4.4×10^{-11}	18
$O(^1D) + H_2O \rightarrow 2\ OH$	2.2×10^{-10}	18
$O(^1D) + O_2 \rightarrow O(^3P) + O_2$	$3.2 \times 10^{-11} \exp(67/T)$	18
$OH + C_6H_6 \rightarrow C_6H_6OH$	$3.8 \times 10^{-12} \exp(-340/T)$	19
$OH + C_6H_6 \rightarrow H_2O + C_6H_5$	$2.7 \times 10^{-16} T^{1.42} \exp(-730/T)$	19
$OH + OH \rightarrow H_2O_2$	$M^a \times 6.2 \times 10^{-31} (T/298)^{-1}$	31
$OH + OH \rightarrow H_2O + O$	$4.2 \times 10^{-12} \exp(-240/T)$	31
$OH + NO \rightarrow HNO_2$	$M^a \times 7.01 \times 10^{-31}(T/298)^{-2.6}$	31
$C_6H_6OH + C_6H_6OH \rightarrow$ products	$6.05 \times 10^{-11}\exp(-236/T)$	this work
$C_6H_6OH + O_2 \rightarrow C_6H_6OH{-}OO$	$1.43 \times 10^{-12} \exp(-2238/T)$	this work
$C_6H_6OH{-}OO \rightarrow C_6H_6OH + O_2$	$1.43 \times 10^{-12}\exp(-2238/T)/K_{c,1}$	this work[b]
$C_6H_6OH + C_6H_6OH{-}OO \rightarrow$ products	$(4.5 \pm 3.5) \times 10^{-10}$	this work

[a] $M = 2.43 \times 10^{19} \times (298/T)$. [b] Based on the rate constant of forward reaction and the equilibrium constant of reaction 1, $K_{c,1}$, used as a fitting parameter (see Table 3).

laser (193.3 nm) photolysis of mixtures $C_6H_6/H_2O/N_2O$/He in a sequence of reactions initiated by the excited oxygen atom, $O(^1D)$:[10]

$$N_2O + h\nu(193\ nm) \rightarrow N_2 + O(^1D) \quad (4)$$

$$O(^1D) + H_2O \rightarrow 2\ OH \quad (5)$$

$$OH + C_6H_6 \rightarrow C_6H_6OH \quad (3a)$$

The quantum yield for production of excited oxygen $O(^1D)$ atoms in the photodissociation of N_2O at 193 nm is equal to one.[18] The rate constants of reactions 5 and 3a at 298 K are 2.2×10^{-10} [18] and 1.2×10^{-12} cm^3 $molecule^{-1}$ s^{-1},[19] respectively. Reaction 3 determines the time scale of the formation of hydroxycyclohexadienyl radicals and limits the apparent time resolution of the kinetic measurements. Under the experimental conditions of this study, the concentration of hydroxycyclohexadienyl radicals reached its maximum within 300 μs.

Reaction Mechanism. The experimental temporal absorption profiles were fitted by a numerical solution of a system of ordinary differential equations, which corresponds to the chosen set of elementary reactions that represents the reaction mechanism. The SCIENTIST software (MicroMath, Inc.) was used to perform the nonlinear least-squares fits by numerical solutions of an ODE system. The rate constants of the reactions used in the modeling are listed in Table 1. Reaction of $O(^1D)$ with benzene is estimated to contribute only ca. 1% of the total sink of excited oxygen atoms and was neglected. Oxygen atoms are produced in photolysis of molecular oxygen at 193 nm. In the current measurements, production of O atoms from the photolysis of O_2 at 193 nm was less than 2.8% of the contribution from the photolysis of N_2O (an estimate based on the ozone yield in the photolysis of molecular oxygen at 193 nm[20]). This contribution was also neglected.

Since the reactions of $O(^1D)$ atoms are much faster than all other reactions listed in Table 1 (at the experimental conditions of this study $O(^1D)$ atoms react within 0.1 μs), they were considered instantaneous. Therefore, the initial concentrations of NO and OH were calculated using the branching ratios listed in Table 1 and used in the model as (variable and fitted) initial conditions.

Results and Discussion

UV Absorption Spectrum and the Cross-Sections of the Hydroxycyclohexadienyl Radical. The measurements of the absorption spectrum of hydroxycyclohexadienyl radicals were performed in two steps. First, the absorption cross-section of the C_6H_6OH radical was measured at the wavelength of 320 nm. Then, the relative absorption spectrum of the C_6H_6OH radical was recorded.

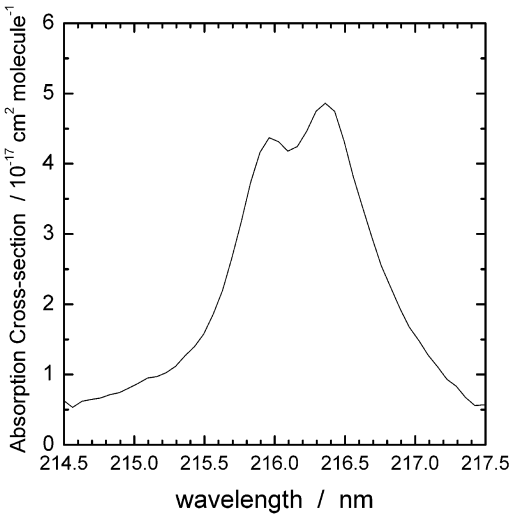

Figure 2. Absorption spectrum of methyl radical around 216 nm (298 K, 1 bar He).

The absorption cross section of the C_6H_6OH radical at 320 nm was measured under conditions when the majority of the OH radicals formed in reaction 5 react with benzene yielding the C_6H_6OH radical in reaction 3a. The temporal profiles of the OH radicals were recorded using a narrow atomic transition line from a Zn hollow cathode lamp at 307.206 nm. The absorption cross-section of the OH radical for this atomic line, 307.206 nm, was determined based on the experimentally measured ratio of the OH and CH_3 radical absorption profiles recorded at 307.206 and 216.509 nm (Cu hollow cathode lamp)[17] and the absorption cross-section of the CH_3 radical at 216.509 nm. The latter value was measured in a separate experiment.

Measurements of the Absorption Cross-Section of the CH_3 Radical at 216.509 nm. Methyl radicals were generated by laser photolysis (193 nm) of acetone vapor in helium:

$$CH_3COCH_3 + h\nu\ (193\ nm) \rightarrow CH_3 + CO + CH_3 \quad (6)$$

This channel accounts for about 95% of the overall photolysis.[21]

The spectrum of the methyl radical was recorded with the time delay of 1 μs after the laser pulse in the range 214−218 nm using the ICCD camera with a 0.027 nm resolution (fwhm with a triangular slit function). Figure 2 shows the absorption spectrum of methyl radical around 216 nm obtained in these experiments. A xenon 75 W arc lamp in the current boosting

mode (60 Amps, 3.0 ms) with a current pulser (MCP 2010, M. U. T., GmbH) served as a source of the monitoring light in this experiments.

The absorption cross-section of CH_3 radical at 216.509 nm was calculated using equation E3:

$$\sigma_{216.509}(CH_3) = \sigma_{app}\,(\sigma_{216.509}(CH_3)/\sigma_{app}) \qquad \text{(E3)}$$

where σ_{app} is an apparent cross-section of the methyl radical at a wavelength of 216.36 nm measured by Macpherson et al.[22] with a 0.6 nm resolution.

The ratio $\sigma_{216.509}(CH_3)/\sigma_{app}$ was calculated from the relative spectra measured in this work using the triangle slit function with the 0.6 nm resolution (fwhm, triangular slit function). Based on the $\sigma_{app} = (4.12 \pm 0.12) \times 10^{-17}$ cm^2 molecule^{-1},[22] the value of $\sigma_{216.509}(CH_3) = (4.20 \pm 0.15) \times 10^{-17}$ cm^2 molecule^{-1} (He, 298 K, 1 bar) was obtained (the errors are one standard deviation).

Measurements of the Absorption Cross-Section of the OH Radical at 307.206 nm. The absorption cross-section of the OH radical at 307.206 nm was determined based on the absorption cross-section of the CH_3 radical at 216.509 nm under the experimental conditions that provide equal initial concentration of both radicals. To provide equal initial concentrations of OH and CH_3 radicals, the reaction of $O(^1D)$ with methane was used:

$$N_2O + h\nu\ (193\ \text{nm}) \rightarrow N_2 + O(^1D) \qquad (4)$$

$$O(^1D) + CH_4 \rightarrow CH_3 + OH \qquad (7a)$$

$$O(^1D) + CH_4 \rightarrow HCHO + H_2 \qquad (7b)$$

The major channel of reaction is channel 7a, which accounts for ca. 90% of the overall reaction of $O(^1D)$ with CH_4. The rate constant for this channel at 298 K is 1.35×10^{-10} cm^3 molecule^{-1} s^{-1}.[18] This mechanism provides equal initial concentrations of methyl and hydroxyl radicals irrespective of the branching ratio of reaction 7 and possible other minor routes of the reaction.

Temporal absorption profiles of OH and CH_3 radicals were recorded with 0.19 nm spectral slit widths at 307.206 and 216.509 nm, respectively. The ratio of the cross-sections ($\sigma_{307.206}(OH)/\sigma_{216.509}(CH_3) = Abs_{307.206}(OH)/Abs_{216.509}(CH_3) = 2.74 \pm 0.11$ at 298 K, 1 bar He), was calculated based on the absorbances of the radicals extrapolated to zero time (the error is one standard deviation).

The absorption cross-section of OH radical at 307.206 nm was determined using expression E4:

$$\sigma_{307.206}(OH) = \sigma_{216.509}(CH_3)(Abs_{307.206}(OH)/Abs_{216.509}(CH_3)) \qquad \text{(E4)}$$

Based on the values of $\sigma_{216.509}(CH_3)$ and $\sigma_{307.206}(OH)/\sigma_{216.509}(CH_3)$, the cross-section of hydroxyl radical at 307.206 nm was determined as:

$$\sigma_{307.206}(OH) = (1.15 \pm 0.06) \times 10^{-16}\ \text{cm}^2\ \text{molecule}^{-1}\ (298\ \text{K, He, 1 bar}) \qquad \text{(E5)}$$

where the error is one standard deviation.

Measurements of the Absorption Cross-Section of the C_6H_6OH Radical at 320 nm. The absorption cross section of C_6H_6OH radical at 320 nm was calculated using the following equation:

$$\sigma_{320}(C_6H_6OH) = \sigma_{307.206}(OH)(Abs_{320}(C_6H_6OH)/Abs_{307.206}(OH))/\alpha \qquad \text{(E6)}$$

where $Abs_{307.206}(OH)$ and $Abs_{320}(C_6H_6OH)$ are the amplitudes of the transient absorptions of OH and C_6H_6OH radicals, respectively, after laser irradiation of the $C_6H_6/H_2O/N_2O$/He mixture with $[C_6H_6] = 5.34 \times 10^{16}$, $[H_2O] = 4.92 \times 10^{17}$, and $[N_2O] = 2.59 \times 10^{16}$ molecule cm^{-3}. The temporal profiles of the C_6H_6OH radical were monitored by the UV absorption at 320 nm with a 1.1 nm resolution (Xe arc with the square pulse current boost technique was used in these experiments). The parameter α in eq E6 is the conversion fraction of OH radicals to C_6H_6OH radicals. At the experimental conditions used in these measurements, the conversion efficiency of $\alpha = 0.87$ was calculated based on the numerical simulation using the reaction mechanism listed in Table 1.

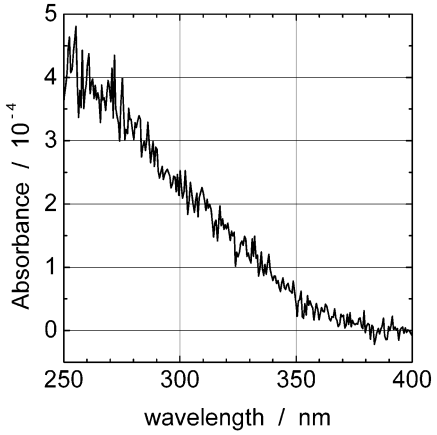

Figure 3. Spectrum of the absorption recorded after 193 nm photolysis of a C_6H_6/N_2O/He mixture. $[C_6H_6]=9.56 \times 10^{15}$, $[N_2O]=1.02 \times 10^{18}$ molecule cm^{-3}, 298 K, 1 bar He.

One of the most significant interfering factors in the spectral and absorption cross-section measurements was the appearance of a time-independent absorption after a 193 nm laser photolysis of mixtures C_6H_6/N_2O/He at wavelengths shorter than 360 nm. The spectrum of the time-independent absorption recorded in the laser photolysis of a C_6H_6/N_2O/He mixture is shown in Figure 3. In this water-free mixture, no C_6H_6OH radicals are formed. It was assumed that the residual absorption is not influenced by the presence of water. To determine the absorption due to the C_6H_6OH radical, the "residual" absorption at 320 nm obtained in the "water-free" experiments was subtracted from the total absorption. The "residual" absorption was determined under the condition when the concentrations of all reactants but water were kept the same. The residual absorption was measured 45 ms after the laser pulse when less than 1% of the maximum concentration of hydroxycyclohexadienyl radicals is left.

The absorption cross section of C_6H_6OH radical at 320 nm was determined based on the procedure and the measurements described above:

$$\sigma_{320}(C_6H_6OH) = (4.37 \pm 0.51) \times 10^{-18}\ \text{cm}^2\ \text{molecule}^{-1} \qquad \text{(E7)}$$

where the error is one standard deviation.

Measurements of the Relative Absorption Spectrum of the Hydroxycyclohexadienyl Radical. The relative absorption spectrum of the hydroxycyclohexadienyl radical was measured using

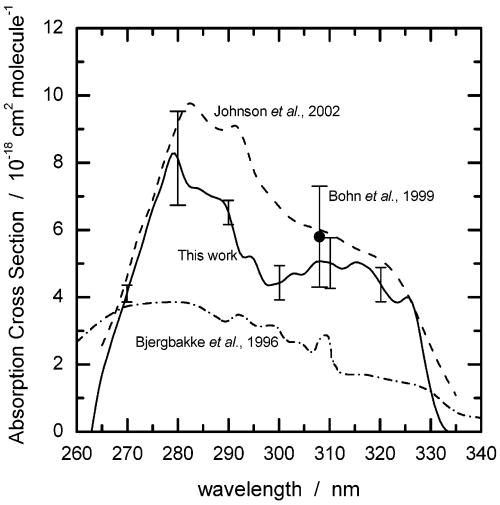

Figure 4. UV absorption spectrum of the C_6H_6OH radical (298 K, 1 bar He).

TABLE 2: UV Absorption Cross Sections of the Hydroxycyclohexadienyl Radical

wavelength/nm	$\sigma(C_6H_6OH)/10^{-18}$ cm^2 molecule^{-1}
270	4.11
275	6.60
280	8.13
285	7.15
290	6.52
295	5.12
300	4.43
305	4.70
310	5.02
315	5.04
320	4.38
325	3.99

the ICCD camera with the 1.1 nm spectral resolution. The transient spectra were recorded with the time gate of 40 μs at the delay of 200 μs after the laser pulse, which corresponds to the maximum concentration of hydroxycyclohexadienyl radicals under the experimental conditions, and at delay of 6 ms after the laser pulse, which correspond to ca. 85% of the radicals consumed due to the self-reaction. The spectrum obtained at 6 ms was subtracted from the spectrum obtained at 200 μs. The difference was used as the relative spectrum of the hydroxycyclohexadienyl radical, under the assumption of the time independence of the interfering "residual" absorption. The relative spectrum was combined with the measured absorption cross-section at 320 nm to yield the absorption cross-sections shown in Figure 4. The cross-section at the absorption maximum, 280 nm, is $\sigma_{280}(C_6H_6OH) = (8.13 \pm 1.40) \times 10^{-18}$ cm^2 molecule^{-1}. The absorption spectrum of the hydroxycyclohexadienyl radical was measured by Bjergbakke et al.[11] Although the wavelength of maximum absorption measured in the present work is in agreement with this determination, there are significant discrepancies both in the shape of the absorption spectrum and in the absorption cross-section at the maximum (Figure 4). The absorption cross-section of $(5.8 \pm 1.5) \times 10^{-18}$ cm^2 molecule^{-1} at 308 nm measured by Bohn et al.[1] is in agreement with the data of the present study (Figure 4, Table 2). Both the spectrum shape and the cross-section in the maximum are in reasonable agreement with the recent results of Johnson et al.:[15] $\sigma_{max,282}(C_6H_6OH) = (10.0 \pm 1.50) \times 10^{-18}$ cm^2 molecule^{-1}, measured relative to the absorption cross-section of $C_2H_5O_2$ radical.

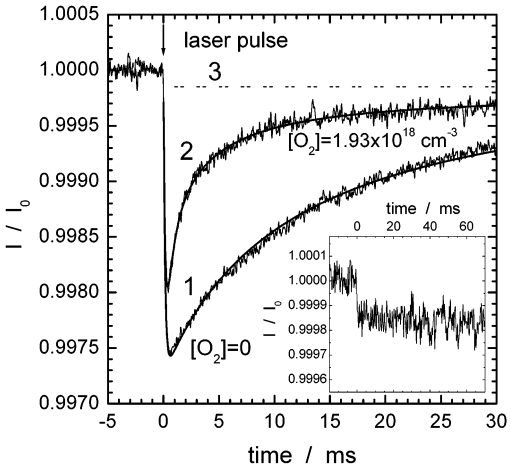

Figure 5. Transient absorption recorded at 315 nm after 193 nm laser pulse without (1) and with molecular oxygen added (2). Dashed line (3): the averaged curve from the insert. Insert: time-independent absorption observed after the laser pulse. The experimental conditions are the same as for curve 2, but $[H_2O] = 0$. (1) $[N_2O] = 1.67 \times 10^{17}$, $[H_2O] = 9.80 \times 10^{16}$, $[C_6H_6] = 6.14 \times 10^{15}$ molecule cm^{-3}. (2) $[O_2] = 1.93 \times 10^{18}$, $[N_2O] = 5.51 \times 10^{17}$, $[H_2O] = 9.04 \times 10^{16}$, $[C_6H_6] = 5.48 \times 10^{15}$ molecule cm^{-3}. 273 K, 1 bar He.

Self-Reaction of Hydroxycyclohexadienyl Radicals. Rate constants of the self-reaction of hydroxycyclohexadienyl radicals (reaction 2) were determined from the temporal absorption profiles acquired in the absence of molecular oxygen. An example of C_6H_6OH radical absorption decay after 193 nm photolysis of a mixture $C_6H_6/H_2O/N_2O$/He is shown in Figure 5 (bottom curve). The absorption profiles were fitted by numerical solutions of a system of ordinary differential equations corresponding to the elementary reactions mechanism listed in Table 1.

TABLE 3: Rate Constant and the Equilibrium Constant for the Reaction of C_6H_6OH with O_2 at Different Experimental Conditions[a]

T/K	$[C_6H_6]/10^{15}$ molecule cm^{-3}	$[N_2O]/10^{17}$ molecule cm^{-3}	$[H_2O]/10^{16}$ molecule cm^{-3}	$[O_2]/10^{18}$ molecule cm^{-3}	$k_1/10^{-16}$ cm^3 molecule^{-1} s^{-1}	$K_{c,1}/10^{-19}$ cm^3 molecule^{-1}
252	6.45	6.40	2.70	0.75	2.13 ± 0.26	15.9
257	6.03	6.31	4.00	1.46	2.18 ± 0.26	17.9
257	5.84	6.11	4.00	2.06	2.27 ± 0.27	12.3
262	5.80	6.02	6.55	2.17	2.80 ± 0.34	4.19
262	5.80	6.02	6.55	2.17	2.96 ± 0.34	4.75
262	5.68	5.54	6.50	1.98	2.65 ± 0.32	7.67
267	5.69	5.91	8.80	2.13	3.17 ± 0.38	5.26
273	5.57	5.78	8.80	2.08	4.31 ± 0.52	2.70
273	5.48	5.51	9.04	1.93	4.00 ± 0.48	3.27
273	5.22	5.44	8.35	3.55	3.60 ± 0.43	3.06

[a]Buffer gas He, 1.01 ± 0.01 bar. The combined errors are shown. Typical initial concentrations of the free radicals were $[O(^1D)]_0 = 7 \times 10^{12}$ molecule cm^{-3}, $[C_6H_6OH]_0 = (1.0-1.5) \times 10^{12}$ molecule cm^{-3}.

TABLE 4: Rate Constants for the C_6H_6OH Radical Self-Reaction at Different Experimental Conditions[a]

T/K	$[C_6H_6]/10^{15}$ molecule cm^{-3}	$[N_2O]/10^{17}$ molecule cm^{-3}	$[H_2O]/10^{16}$ molecule cm^{-3}	$k_2/10^{-11}$ cm^3 molecule^{-1} s^{-1}
252	6.51	6.77	2.70	2.28 ± 0.52
262	6.35	8.70	7.00	2.65 ± 0.60
262	6.33	6.33	8.67	2.53 ± 0.58
273	6.14	1.67	9.80	2.31 ± 0.52
285	5.62	5.48	9.23	2.74 ± 0.62

[a] Buffer gas He, 1.01 ± 0.01 bar.

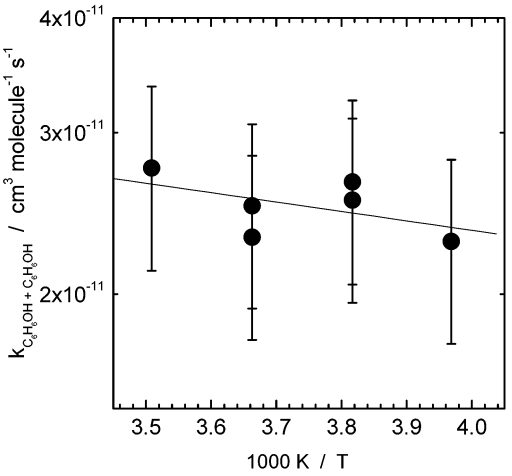

Figure 6. Arrhenius plot for the self-reaction of C_6H_6OH radicals.

The Arrhenius plot for k_6 is shown in Figure 6. The self-reaction of hydroxycyclohexadienyl radicals has a weak temperature dependence:

$$k_2 = (6 \pm 3) \times 10^{-11} \exp(-2.0 \pm 1.6 \text{ kJ mol}^{-1}/RT) \text{ cm}^3 \text{ molecule}^{-1} \text{ s}^{-1} \quad \text{(E8)}$$

In the middle of the temperature range studied, 252−285 K, $k_2(267) = (2.5 \pm 0.4) \times 10^{-11}$ cm^3 molecule^{-1} s^{-1}. The Arrhenius expression extrapolated to 298 K yields $k_2(298) = 2.77 \times 10^{-11}$ cm^3 molecule^{-1} s^{-1} in agreement (within the experimental accuracy) with $k_2(298) = (3.4 \pm 1.7) \times 10^{-11}$ cm^3 molecule^{-1} s^{-1} obtained by Bohn et al.[1]

Kinetics of the Hydroxycyclohexadienyl Radical in the Presence of O_2. The decay kinetics of the hydroxycyclohexadienyl radical in the presence of O_2 was studied over the temperature range 252−298 K. At temperatures above 285 K, the kinetic profiles can be fitted by a single-exponential decay function. At temperatures below 273 K, two-time-domain kinetic profiles were observed. An example of such a two-time-domain kinetic profile observed at 273 K in the presence of molecular oxygen is shown in Figure 5 (curve 2). The observed decays were interpreted in terms of establishing of pseudo-equilibrium in reaction 1. The first (fast) part of the kinetic curves was attributed to the "equilibration" $C_6H_6OH + O_2 \rightleftharpoons C_6H_6OH-OO$. The subsequent slower decay was interpreted as being due to the radical−radical reactions and to the further unimolecular transformation of the peroxy adduct C_6H_6OH-OO as well as in reactions with O_2. As the temperature increases, the equilibrium shifts toward the reactants, the hydroxycyclohexadienyl radical and molecular oxygen, and cannot be observed at temperatures above 285 K using the concentrations of molecular oxygen of the current study.

There exists a small "residual" absorption (Figure 5, insert) that survives at long times after all radical reactions are completed. The magnitude of this residual absorption is proportional to the laser pulse energy and benzene concentration. The residual absorption was attributed to the products of benzene photolysis. The amplitude of the residual absorption was assessed using photolysis of a mixture $C_6H_6/N_2O/O_2/He$ (without water, the source of OH radicals) at 193 nm (Figure 5, insert). The magnitude of the residual absorption determined in this way was used in the numerical fitting of the experimental kinetic curves. This absorption does not depend on temperature over the range 252−273 K.

The origin of the residual absorption is not clear. It was reported that in the photolysis of benzene in the gas phase at 160−200 nm[23] and at 185 nm[24] the major product is an isomer of benzene, fulvene, which has a characteristic absorption at 235 nm. In the photolysis of $C_6H_6/N_2O/He$ mixtures at 193 nm, we observed permanent (time independent) continuous absorption in the range of 210−360 nm which does not exhibit any fine structure. However, this absorption is centered near 245 nm. It is possible that in the presence of N_2O in addition to fulvene other stable products are formed. The important assumption for the data processing is the time independence of this residual absorption. It was also assumed that addition of water does not affect the amplitude of this absorption.

The measurements of C_6H_6OH radical kinetics were performed at the concentrations of molecular oxygen in the range of $7.5 \times 10^{17}-3.6 \times 10^{18}$ molecule cm^{-3} over the temperature range 252−273 K. To extract the equilibrium constants the experimental absorption temporal profiles were processed by a numerical fitting using the reaction mechanism listed in Table 1. In the fits, four fitting parameters were used: the photon flux, the rate constant of reaction 1, the equilibrium constant of reaction 1, and the rate constant of the cross-reaction between hydroxycyclohexadienyl radicals and hydroxycyclohexadienyl peroxy radicals. Other rate constants were fixed at the values listed in Table 1. The rate constant of the self-reaction of hydroxycyclohexadienyl radicals (reaction 2) was determined separately in the experiments without molecular oxygen added. It was assumed that the peroxy radical formed ($C_6H_6OH(OO)$) does not absorb at the monitoring wavelength, 320 nm. Attempts to locate and to measure the absorption of the peroxy radical were unsuccessful.

Theoretical calculations[16] indicate the existence of four isomers of the hydroxycyclohexadienyl peroxy radical (ortho (E) and (Z) and para (E) and (Z), (E) and (Z) refer to the mutual position of H-atom in the hydroxyl group and O-atom in the −O−O fragment relative to the ring plane) with comparable bond energies, the (E)-ortho isomer (the H-atom and O-atom on the opposite sides of the ring) being the most stable one. The bond energies for these isomers differ by ca. 10 kJ mol^{-1}, and all of them could play a role in the equilibration kinetics. However, it is impossible to resolve these isomers based on the currently available experimental data. In the processing of the kinetic data, all of the bound isomers were lumped in a single species. The modified van't Hoff plot[25,26] for the equilibrium constant of reaction 1, $C_6H_6OH + O_2 \rightleftarrows C_6H_6OH-OO$, is shown in Figure 7:

$$\ln(K) + \text{correction} = -\Delta H^\circ_{298}/RT + \Delta S^\circ_{298}/R \quad \text{(E9)}$$

In this equation the "correction" is

$$\text{correction} = -\Delta(\delta S^\circ_{T,298})/R + \Delta(\delta H^\circ_{T,298})/RT \quad \text{(E10)}$$

$$\delta S^\circ_{T,298} = S^\circ_T - S^\circ_{298}; \quad \delta H^\circ_{T,298} = H^\circ_T - H^\circ_{298} \quad \text{(E11)}$$

The correction term in the modified van't Hoff expression E9

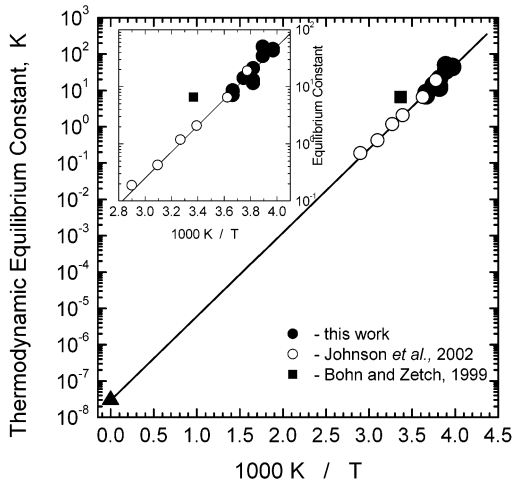

Figure 7. Van't Hoff plot for reaction 1 ($C_6H_6OH + O_2 \leftrightarrow C_6H_6$-$OH-O_2$).

could be calculated based on the difference of the heat capacities of the reactants and the products of the reaction, ΔC_p, which is convenient for estimates:

$$\text{correction} = (1/R)\int_{298}^{T}\Delta C_p(T')[1/T - 1/T']\,dT' \quad \text{(E12)}$$

A conservative estimate on the ΔC_p in reaction 1, $\Delta C_{p,1} < 2$ R, implies that at the middle temperature of the temperature range (263 K) used in the study, the correction term in eq E9 is rather small, |"correction"| < 0.015. This leads to the maximum error in the standard enthalpy of reaction 1 caused by neglecting the correction of ca. 0.03 kJ mol^{-1}. Therefore, the correction term in eq E9 was neglected in the data processing.

In the modified van't Hoff plot (Figure 7), the thermodynamic equilibrium constant (dimensionless, standard pressure 1 bar) is plotted vs the inverse temperature. The point at $1/T = 0$ is obtained using the calculated standard entropy of reaction 1. Based on the estimated thermodynamic properties (Lay et al.[2]), ΔS°_{298}(reaction 1) = −136 J mol^{-1} K^{-1}. The ab initio calculations of Johnson et al.[15] yielded ΔS°_{298}(reaction 1) = −160 J mol^{-1} K^{-1}. The two published calculated values for the standard entropy change in reaction 1 differ significantly. The recent ab initio calculations of Chen and Bozzelli[16] yielded an intermediate value: ΔS°_{298}(reaction 1) = −142 J mol^{-1} K^{-1} assuming the equilibrium mixture of two enantiomers of the peroxy radical. The uncertainty in the standard entropy of reaction 1 has an impact on the standard enthalpy of this reaction determined from the equilibrium constant in the third law determination. From the equilibrium constants measured in this work, a value of $\Delta H^\circ_{1,298} = -(42.5 \pm 2.0)$ kJ mol^{-1} was derived using the third law method with $\Delta S^\circ_{1,298} = -136$ J mol^{-1} K^{-1} estimated by Lay et al.[2]. Using the value of Johnson et al.,[15] $\Delta S^\circ_{1,298} = -160$ J mol^{-1} K^{-1}, leads to $\Delta H^\circ_{1,298} = -(48.1 \pm 2.0)$ kJ mol^{-1}. Finally, the recently calculated intermediate value of $\Delta S^\circ_{1,298} = -141.6$ J mol^{-1} K^{-1} (Chen and Bozzelli[16]) results in $\Delta H^\circ_{1,298} = -(43.6 \pm 2.0)$ kJ mol^{-1}. In the earlier work,[2] the reaction entropy was estimated based on the group contributions, the value is not expected to be accurate. The discrepancy between the theoretical values of Johnson et al.[15] and Chen and Bozzelli[16] originates from the entropy of the peroxy radical. The structural parameters as well as the vibrational frequency of the peroxy radical are in excellent agreement in both calculations. In the paper of Johnson et al., a rigid-rotor-harmonic oscillator approximation was used in application to all degrees of freedom, including the hindered rotations about the C−O bond in the C−O−O fragment as well as about the C−O bond in the C−O−H fragment. More accurate treatment based on the calculated hindrance potentials using the method developed for the arbitrary hindrance potential[27] yields higher entropy of these two modes by 7.7 J mol^{-1}K^{-1}.

In addition, two enantiomers (each having two optical isomers) of the (*E*)-*o*-CHD-OH−OO isomer were taken into account. These two enantiomers both have OH and OO groups on the opposite side of the ring. The second enantiomer is obtained from the first one by interchanging the OH and OO groups with the adjacent hydrogen atoms. Although the most stable enantiomer is one that has a hydrogen bond between the H atom from OH group and the O atom in the OO group, the second enatiomer has enthalpy higher by only 7.4 kJ mol^{-1}. In addition, due to the absence of the hydrogen bonding in this enantiomer, it has higher entropy.

These two contributions (accounting for equilibrium mixture of two enantiomers as well as treating torsional modes C−OH and C−OO as hindered rotors) account for the whole difference in the reaction entropies. Because of these reasons, the most recent value of the standard entropy of reaction 1 was accepted in the third law determinations.

A reliable estimate of the uncertainty of the calculated standard entropy of reaction 1 is difficult. There is the error cancellation from the contributions of the similar vibrations in the reactant and the product radicals in reaction 1. The main uncertainty arises from the newly formed loose degrees of freedom, specifically from the two hindered rotations. The possible error in the reaction entropy was estimated as ±2 J mol^{-1} K^{-1}, which leads to an additional uncertainty in the reaction enthalpy determined using the third method of ±0.5 kJ mol^{-1}.

The equilibrium constants measured in this work agree well with these determined by Johnson et al.[15] from the absorption amplitude depression by molecular oxygen (Figure 7). A single-temperature measurement of Zetzsch and co-workers[1] is higher than that obtained in this work as well as in the measurements of Johnson et al. by a factor of 3.4.

The experimentally determined R−OO bond energy in hydroxycyclohexadienyl peroxy radical, $DH^\circ_{C_6H_6(OH)-O_2} = 43.6 \pm 2.0$ kJ mol^{-1} can be compared with the recent ab initio calculations, 51 [15] and 56 kJ mol^{-1}.[16] It should be stressed again that both the experiments performed in this work and in the previous studies cannot distinguish between the four possible isomers of hydroxycyclohexadienyl peroxy radical, which should be taken into account when comparing the experimental results with the theoretical calculations.

The reaction mechanism used to fit the experimental profiles does not include the hypothetical irreversible loss of hydroxycyclohexadienyl peroxy radical in reaction with molecular oxygen. This reaction was introduced by Bohn et al.[1,28] and, later, Johnson et al.[15] to fit their data. Their fits required quite slow (2×10^{-16} cm^3 molecule^{-1} s^{-1} [1,28] and $(5.5 \pm 0.6) \times 10^{-16}$ cm^3 molecule^{-1} s^{-1})[15] but temperature independent additional reaction (beyond reaction 1) of the hydroxycyclohexadienyl radical with molecular oxygen which leads to irreversible losses of the radical pool. The low value of the rate constant for this hypothetical reaction is not consistent with the temperature independence. In the data processing of this work, it was found that the profiles could be fitted without inclusion of such reaction provided the reaction of the hydroxycyclohexadienyl radical with its peroxy radical is fast (Table 1). For comparison, the reaction of methyl radicals with methyl peroxy is fast, ca. 1×10^{-10} cm^3 molecule^{-1} s^{-1}.[29] Essentially, a

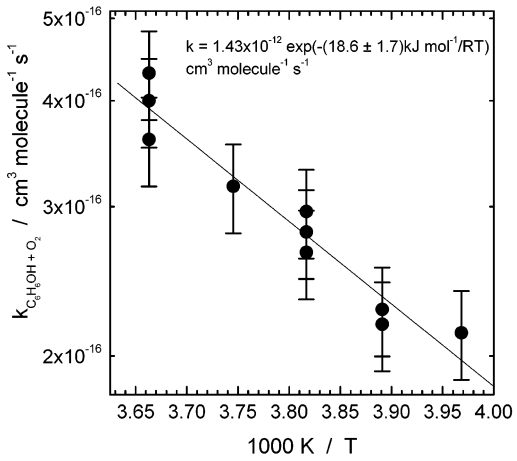

Figure 8. Arrhenius plot for the reaction $C_6H_6OH + O_2 \rightarrow C_6H_6OH-O_2$.

reaction, that leads to depletion of the radical pool either via an "irreversible side reaction" of the reactant hydroxycyclohexadienyl radical or the product hydroxycyclohexadienyl peroxy radical with molecular oxygen or a fast cross-reaction of these radicals, is required to fit the experimental profiles. Analysis shows that the cross-reaction of hydroxycyclohexadienyl radical with its peroxy ("k_{cross}") under the pseudo-equilibrium conditions can mimic a bimolecular reaction of hydroxycyclohexadienyl radical with molecular oxygen ("k_{loss}"). An estimate for the cross-reaction rate constant, k_{cross}, based on the rate constant of the reaction of irreversible loss of hydroxycyclohexadienyl radical with molecular oxygen, k_{loss}, can be obtained: $2k_{cross} \approx k_{loss}[O_2]/[C_6H_6OH]_0$. Using $k_{loss} = 5.5 \times 10^{-16}$ cm^3 molecule^{-1} s^{-1}, $[O_2] = 2 \times 10^{19}$ molecule cm^{-3}, and $[C_6H_6OH]_0 = 2.6 \times 10^{13}$ molecule cm^{-3} [15] leads to $k_{cross} = 2 \times 10^{-10}$ cm^3 molecule^{-1} s^{-1}, which is consistent with the current work.

However, the success of the fits of the concentration profiles without taking into account an irreversible side reaction does not rule out its existence. The actual situation could be that both reactions play a role and their relative importance depends on the concentration of free radicals. In the study of Bohn and Zetch (at a single temperature), lower initial concentrations of free radical were employed (ca. 2×10^{11} molecule cm^{-3} [1]). This study required the lowest rate constant for the "side reaction" to fit the data ($k_{loss} = 2.1 \times 10^{-16}$ cm^3 molecule^{-1} s^{-1}). In the two studies where temperature dependence was measured (and temperature independence of the loss reaction was observed) higher concentrations were used (ca. 1×10^{12} molecule cm^{-3} in the current study and ca. 3×10^{13} molecule cm^{-3} in the study of Johnson et al.[15]). It could be noted that the rate constant of the side reaction required to fit the data in the study of Johnson et al. is 2.6 times higher, $k_{loss} = 5.5 \times 10^{-16}$ cm^3 molecule^{-1} s^{-1}.

Currently, the availability and the quality of the kinetic data required for the mechanism of the reaction are insufficient to resolve this issue. The model fits of the experimental profiles obtained in this study using the mechanism that includes the irreversible loss reaction demonstrated insensitivity of the extracted equilibrium constant toward the inclusion or exclusion of this reaction in the mechanism.[30]

Together with the equilibrium constants, the fits of the temporal profiles of the hydroxycyclohexadienyl radical resulted in the rate constants of reaction of the hydroxycyclohexadienyl radical with molecular oxygen (reaction 1). The Arrhenius plot for this reaction is shown in Figure 8. The temperature dependence of the rate constant is

$$k_1 = (1.4 \pm 0.8) \times 10^{-12} \exp(-(18.6 \pm 1.7)\ \text{kJ mol}^{-1}/RT)\ \text{cm}^3\ \text{molecule}^{-1}\ \text{s}^{-1} \quad \text{(E13)}$$

There are several recent studies in which rate constant of reaction 1 was reported. The measured rate constants of this reaction ($k_1 = (1.8 \pm 0.5) \times 10^{-16}$ at 298 K,[9] $(5.0 \pm 1.0) \times 10^{-13}$ at 338 K,[11] and $(2 \pm 1) \times 10^{-15}$ at 297 K[1] (cm^3 molecule^{-1} s^{-1} units)) differ by 3 orders of magnitude. Extrapolation of the temperature dependence of k_1 obtained in this work to 297 K yields $k_1(297) = 7.6 \times 10^{-16}$ cm^3 molecule^{-1} s^{-1}, reasonably close to the estimates of Bohn et al. The high value reported by Bjergbakke et al.[11] $k_1(338) = (5.0 \pm 1.0) \times 10^{-13}$ cm^3 molecule^{-1} s^{-1} is in a large discrepancy (by a factor of 260) with the result of this and previous works (eq E13 extrapolated to 338 K yields 1.91×10^{-15} cm^3 molecule^{-1} s^{-1}).

Conclusion

UV spectroscopy and the kinetics of the hydroxycyclohexadienyl radical were studied using laser photolysis−transient absorption spectroscopy using a multipass cell of a novel design. The UV absorption cross-sections of the hydroxycyclohexadienyl radical were determined. Both the shape and the maximum cross-section of the spectrum differ significantly from these reported by Bjerbakke et al.[11] The cross-section is in agreement with a single wavelength measurement (308 nm) of Bohn et al.[1] and recent measurements of Johnson et al.[15] The rate constant of self-reaction of hydroxycyclohexadienyl radical was determined over the temperature range 252−285 K. Quasi-equilibrium in the reaction of hydroxycyclohexadienyl radicals with molecular oxygen was studied over the temperature range 252−273 K. Modeling of the experimental profiles using a small reaction mechanism yielded the rate constant as well as the equilibrium constant of reaction 1. The equilibrium constants are in excellent agreement with the recent measurements of Johnson et al.[15] The equilibrium constants were used to determine the standard enthalpy of reaction 1, based on the third law using the theoretical entropy of reaction 1.

Acknowledgment. This research was supported by a grant from the MIT/NJIT/Caltech USEPA Center on Airborne Organics.

Appendix: The Multipass Cell

An optically stable cavity formed by two highly reflective mirrors is illuminated by a "parallel" aperture-formed beam of light from one end. The intensity of the light emerging from the opposite end of the cavity is measured. In the analysis below, two major assumptions were made.

(i) It is assumed that the beam is formed in such a way to prevent excitation of very high order transverse modes of the cell, so that the diffraction losses are negligible compared to the other losses of the cell. This assumption implies that all excited modes of the cell have equal losses determined by the mirror losses and absorption by the medium inside the cell.

(ii) It is also assumed that the number of the excited modes of the cavity is large, so that the coherent effects are not important, and the treatment based on light intensity (or photon flux) is applicable.

Let I_{inc} and I be the incident and outlet light intensities, respectively, τ_1 and τ_2 are the mirrors transmittances, r_1 and r_2 are the mirrors reflectivities, and τ is the one-pass medium attenuation coefficient. The output light intensity then is given

by the sum in eq A1:

$$I = I_{inc}\,\tau_1\tau_2\tau\,(1 + r_1r_2\tau^2 + (r_1r_2\tau^2)^2 + (r_1r_2\tau^2)^3 + (r_1r_2\tau^2)^4 + ...) \quad (A1)$$

The series A1 (a geometrical progression) is easily summed:

$$I = I_{inc}\,\tau_1\tau_2\tau/(1 - r_1r_2\tau^2) \quad (A2)$$

Introducing the cell "gain"

$$\text{Gain} = (1/\text{I})\,(\text{d}I/\text{d}\tau) \quad (A3)$$

one obtains

$$\text{Gain} = (1/\tau)(1 + r_1r_2\tau^2)/(1 - r_1r_2\tau^2) \quad (A4)$$

Assuming high reflectivity mirrors and low one pass loss of the medium

$$1 - r_{1,2} \ll 1; \quad 1 - \tau \ll 1 \quad (A5)$$

and introducing the average one-pass loss of the cell

$$\text{One Path Loss} = (1 - r_1)/2 + (1 - r_2)/2 + 1 - \tau \quad (A6)$$

one derives from eq A4

$$\text{Gain} = (\text{One Pass Loss})^{-1} \quad (A7)$$

Expression A7 shows the enhancement in the light intensity modulation by an additional small absorption (Abs) compared to the light intensity modulation in the one-pass arrangement provided that the additional absorption is small in comparison with the average one-pass loss of the cell:

$$\text{Abs} \ll \text{One Pass Loss} \quad (A8)$$

$$\delta I/I_0 = \text{Gain}(\delta I/I_0)_{\text{OnePass}} \quad (A9)$$

If the criterion A8 is not fulfilled and the additional absorption is comparable with the one pass cavity loss, eq A9 cannot be used. When additional absorption is comparable with the one pass loss, the light intensity change is comparable with the initial light intensity in the absence of absorption. However, if the additional absorption is still small, Abs $\ll$ 1, equation A2 can be transformed as

$$I = I_0/(1 + \text{Abs Gain}_0) \quad (A10)$$

where I_0 and Gain_0 are the output light intensity and the cell gain in the absence of the additional absorption, respectively. To convert the light intensity into the absorption, eq A10 should be rearranged as follows:

$$\text{Abs} = (1 - I_0/I)/\text{Gain}_0 \quad (A11)$$

For practical purposes, an additional parameter of the cell, the "contrast", is of interest. The "contrast", *C*, is defined as the ratio of the light intensity of an aligned cell and the light intensity emerging from a completely misaligned cell (only one pass possible). The light intensity for a misaligned cell is given by the first term in the series A1

$$I_{\text{detuned}} = I_{\text{inc}}\tau_1\tau_2\tau \quad (A12)$$

Therefore, the cell contrast is

$$C = I/I_{\text{detuned}} = 1/(1 - r_1r_2t^2) \quad (A13)$$

For a low one pass loss cell this is transformed to

$$C = \text{Gain}/2 \quad (A14)$$

The attenuation of the incident light by the cell is obtained from eq A2. Assuming no additional losses on the mirrors, $\tau_1 = 1 - r_1$, $\tau_2 = 1 - r_2$, and a transparent medium, $\tau = 1$, one derives

$$I/I_{\text{inc}} = \tau_1\tau_2/(\tau_1 + \tau_2) \quad (A15)$$

If the mirrors have equal reflectivities, $\tau_1 = \tau_2$, eq. A13 becomes

$$I/I_{\text{inc}} = \tau_1/2 \quad (A16)$$

This expression has a very simple interpretation. Only a fraction of τ_1 of all incident photons penetrate inside the cavity. After that, a photon has equal chances to leave the cell through either mirror, which additionally halves the light intensity.

To illustrate the above expressions, a cell made of two perfect mirrors with 98% reflectivity and perfectly matched with the incident beam is considered. For such a cell, the one pass loss is 2%, the theoretical gain is 50, and the theoretical contrast is 25. A detuned cell will attenuate the monitoring light 2500 times, and an aligned cell will attenuate the monitoring light only 100 times. Only 2% of the incident photons penetrate inside the cell. Half of these photons leave through the second mirror. Photons make a different number of passes in the cell, but on average, photons make 50 passes. If the absorption to be monitored is much less than 2%, than eq A9 can be used. If the absorption is comparable with 2%, but still small, eq A11 should be used to convert the light intensity into the absorption.

References and Notes

(1) Bohn, B.; Zetzsch, C. *Phys. Chem. Chem. Phys.* **1999**, *1*, 5097.
(2) Lay, T. H.; Bozzelli, J.W.; Seinfeld, J. H. *J. Phys. Chem.* **1996**, *100*, 6543.
(3) Atkinson, R.; Aschmann, S. M. *Int. J. Chem. Kinet.* **1994**, *26*, 929.
(4) Atkinson, R.; Aschmann, S. M.; Arey, J.; Carter, W. P. L. *Int. J. Chem. Kinet.* **1989**, *21*, 801.
(5) Semadeni, M.; Stocker, D. W.; Kerr, J. A. *Int. J. Chem. Kinet.* **1995**, *27*, 287.
(6) Wallington, T. J.; Neuman, D. M.; Kurylo, M. J. *J. Int. Chem. Kinet.* **1987**, *19*, 725.
(7) Perry, R. A.; Atkinson, R.; Pitts, J. N., Jr. *J. Phys. Chem.* **1977**, *81*, 296.
(8) Witte, F.; Urbanik, E.; Zetzsch, C. *J. Phys. Chem.* **1986**, *90*, 3251.
(9) Knispel, R.; Koch, R.; Seise, M.; Zetzsch, C. *Ber. Bunsen-Ges. Phys. Chem.* **1990**, *94*, 1375.
(10) Lin, S.-C.; Kuo, T.-C.; Lee, Y.-P. *J. Chem. Phys.* **1994**, *101*, 2098.
(11) Bjergbakke, E.; Sillesen, A.; Pagsberg, P. J. *J. Phys. Chem.* **1996**, *100*, 5729.
(12) Zellner, R.; Fritz, B.; Priedel, M. *Chem. Phys. Lett.* **1985**, *121*, 412.
(13) Ghigo, G.; Tonachini, G. *J. Am. Chem. Soc.* **1998**, *120*, 6753.
(14) Ghigo, G.; Tonachini, G. *J. Am. Chem. Soc.* **1999**, *121*, 8366.
(15) Johnson, D.; Raoult, S.; Rayez, M.-T.; Rayez, J.-C.; Lesclaux, R. *Phys. Chem. Chem. Phys.* **2002**, *4*, 4678.
(16) Chen, C.; Bozzelli, J. W. to be published.
(17) Krasnoperov, L.; Mehta, K. *J. Phys. Chem. A* **1999**, *103*, 8008.
(18) Atkinson, R.; Baulch, D. L.; Cox, R. A.; Hampson, R. F.; Kerr, J. A.; Rossi, M. J.; Troe, J. *J. Phys. Chem. Ref. Data* **1997**, *26*, 521.
(19) Baulch, D. L.; Cobos, C. J.; Cox, R. A.; Esser, C.; Frank, P.; Just, Th.; Kerr, J. A.; Pilling, M. J.; Troe, J.; Walker, R. W.; Warnatz, J. *J. Phys. Chem. Ref. Data* **1992**, *21*, 411.
(20) Krasnoperov, L. N.; Stepanov, V. *J. Chem. Educat.* **1999**, *76*, 1182.
(21) Lightfoot, P. D.; Kirwan, S. P.; Pilling, M. J. *J. Phys. Chem.* **1988**, *92*, 4938.
(22) Macpherson, M. T.; Pilling, M. J.; Smith, M. J. C. *J. Phys. Chem.* **1985**, *89*, 2268.
(23) Ward, H. R.; Wishnok, J. S.; Sherman, P. S. *J. Am. Chem. Soc.* **1967**, *89*, 162.

(24) Kaplan, L.; Wilzbach, K. E. *J. Am. Chem. Soc.* **1967**, *89*, 1030.

(25) Benson, S. W. *Thermochemical Kinetics*, 2nd ed.; Wiley: New York, 1976.

(26) Morgan, C. A.; Pilling, M. J.; Tulloch, J. M.; Ruiz, R. P.; Bayes, K. D. *J. Chem. Soc., Faraday Trans. 2.* **1982**, *78*, 1323.

(27) Lay, T. H.; Krasnoperov, L. N.; Venanzi, C. A.; Bozzelli, J. W.; Shokhirev, N. V. *J. Phys. Chem.* **1996**, *100*, 8240.

(28) Bohn, B. *J. Phys. Chem. A* **2001**, *105*, 6092.

(29) Mallard, W. G.; Westley, F.; Herron, J. T.; Hampson, R. F. NIST Chemical Kinetics Database, ver. 6.01. NIST Standard Reference Data; INST: Gaithersburg, MD, 1994.

(30) Bohn, B. Personal communication, 2002.

(31) DeMore, W. B.; Sander, S. P.; Golden, D. M.; Hampson, R. F.; Kurylo, M. J.; Howard, C. J.; Ravishankara, A. R.; Kolb, C. E.; Molina, M. J. *Chemical Kinetics and Photochemical Data for Use in Stratospheric Modeling. Evaluation number 12*; Jet Propulsion Laboratory: Pasadena, CA, 1997.